

Origin of the double-peaked narrow emission-lines in the optical spectra of X-shaped Radio Galaxies

PRAJNADITY GHOSH ¹, RAVI JOSHI ¹, XIAOLONG YANG ², YINGKANG ZHANG ², GOPAL-KRISHNA,³ PAUL J. WIITA ⁴, ANKIT PATEL ¹,
ARTI GOYAL ⁵, GOURAB GIRI ⁶, SANTANU MONDAL ¹, VIBHORE NEGI ⁷, MAREK WEZGOWIEC ⁵, XUE-BING WU ^{7,8} AND LUIS C. HO ^{7,8}

¹Indian Institute of Astrophysics (IIA), Koramangala, Bangalore, 560034; India

²Key Laboratory for Research in Galaxies and Cosmology, Shanghai Astronomical Observatory, Chinese Academy of Sciences, 80 Nandan Road, Shanghai 200030, People's Republic of China

³UM-DAE Centre for Excellence in Basic Sciences (CEBS), Vidyasagar, Mumbai, 400098, India

⁴Department of Physics, The College of New Jersey, 2000 Pennington Road, Ewing, NJ 08628-0718, USA

⁵Observatorium Astronomiczne Uniwersytetu Jagiellońskiego, ul. Orla 171, 30-244 Kraków, Poland

⁶Istituto Nazionale di Astrofisica (INAF) – Istituto di Radioastronomia (IRA), via Gobetti 101, 40129 Bologna, Italy

⁷Kavli Institute for Astronomy and Astrophysics, Peking University, Beijing 100871, People's Republic of China

⁸Department of Astronomy, School of Physics, Peking University, Beijing 100871, People's Republic of China

ABSTRACT

We investigate the X-shaped radio galaxies (XRGs) with optical double-peaked narrow emission (DPNEL) as potential hosts of dual or binary supermassive black holes (SMBHs). Using a sample of 187 XRGs selected from SDSS and DESI optical spectroscopic surveys, we check the AGN nature of both emission components using the BPT diagnostics of multiple emission lines, namely [O III] $\lambda\lambda 4959, 5007$, H α , [N II] $\lambda\lambda 6548, 6584$, [S II] $\lambda\lambda 6716, 6731$, and H β , and mid-infrared colors. We find that the detection rate of [O III] DPNEL features in XRGs is 30% compared to just 1% in the general galaxy population (mostly radio quiet). The dual AGN fraction in DPNEL galaxies is found to depend strongly on the radio luminosity, increasing from $\sim 25\%$ for radio-undetected to $\sim 58\%$ in the radio-detected sample of general DPNEL galaxies. In contrast, the DPNEL XRGs and FR-II radio galaxies having higher radio power show a $\sim 95\%$ likelihood of hosting a dual AGN. Secondly, the detection of companion galaxies in more than 30% of DPNEL XRGs suggests a vital role of mergers in the XRG formation. We also investigate the parsec-scale radio structure of the nuclei of several XRGs using Very Long Baseline Array (VLBA) maps at 1.4 GHz, 4.3 GHz or 7.6 GHz and find a resolved core for only one of the XRGs. However, the flat spectral indices of the VLBA cores along with the DPNEL components exhibiting AGN characteristics, together with the detection of radio-optical offsets between the VLBA and Gaia position, are strongly indicative of XRGs being likely candidates for hosting dual/binary AGNs.

Keywords: Galaxies (573) — Active Galaxies (17) — Active Galactic Nuclei (16) — Radio jets (1347) — Supermassive Black Holes (1663) — Radio Galaxies (1343)

1. INTRODUCTION

In the hierarchical model of galaxy evolution, mergers play a dominant role in the final evolutionary stages (S. D. M. White & M. J. Rees 1978; G. Kauffmann & M. Haehnelt 2000). In the course of a merger, the central supermassive black holes (SMBHs) from each progenitor galaxy may form a close pair within the remnant galaxy (e.g. S. Komossa 2006). If both merging galaxies are gas-rich, substantial amounts of gas are funneled into their central regions, simultaneously triggering black hole accretion, and initiating a central starburst (L. Hernquist 1989; P. F. Hopkins et al. 2006a; J. M. Comerford et al. 2015). This stage, characterized by two SMBHs actively accreting within the same

galaxy at kiloparsec-scale separations, is known as the *dual* active galactic nuclei (*dual* AGN) phase.

As the merger progresses, dynamical friction causes the SMBHs to lose energy, bringing them from kiloparsec to parsec-scale separations (M. C. Begelman et al. 1980). Under favorable conditions, the two black holes enter a gravitationally bound orbital configuration (M. Volonteri et al. 2003), leading to the *binary* AGN phase. Eventually, gravitational wave emission dominates their energy loss, culminating in coalescence — an event detectable by future space-based gravitational wave observatories such as the Laser Interferometer Space Antenna (LISA; P. Amaro-Seoane et al. 2017).

Detecting dual and binary AGNs is the key to understanding the co-evolution of SMBHs, the fueling of AGN driven by galaxy mergers, and the formation of gravitational wave sources (see [A. De Rosa et al. \(2019\)](#) and references therein). Cosmological and merger simulations suggest that the occurrence of dual AGNs correlates with the galaxy merger rate, which peaks around cosmic noon ($z \sim 1-3$), where the corresponding dual AGN fraction is $\leq 6\%$ ([C. Puerto-Sánchez et al. 2025](#)). Further simulations indicate that for a sample of major and minor mergers hosting dual AGN, the fraction is 20-30% and 1-10% respectively ([P. R. Capelo et al. 2017](#)). Despite these theoretical expectations, dual AGNs remain quite rare from an observational perspective ([K. Rubinur et al. 2017](#); [Y.-W. Zhang et al. 2021](#)), conceivably due to challenges such as dust obscuration, AGN duty cycle, short lifetimes of the dual AGN phase, and limitations imposed by the required resolution of micro-arcseconds. In the recent Big Multi-AGN Catalog (Big MAC) ([R. W. Pfeifle et al. 2024](#)), a total of 156 confirmed dual AGN systems have been identified using techniques including optical spectroscopy, radio, and mid-infrared imaging; a further 4180 dual AGN candidates have been cataloged from the literature. In contrast, due to the requirement for parsec-scale resolution, only one ([C. Rodriguez et al. 2006](#)) confirmed binary AGNs have been discovered, while approximately 1368 candidates are listed in Big MAC. Since direct detection methods such as high-resolution imaging in the X-ray ([M. Hou et al. 2019](#)), optical ([M. Imanishi & Y. Saito 2014](#); [X. Liu et al. 2018](#); [A. Bhattacharya et al. 2023](#)), radio bands ([K. Rubinur et al. 2019](#); [E. Schwartzman et al. 2024](#)) and Integral Field Spectroscopy (IFS) ([M. Perna et al. 2023](#); [M. Scialpi et al. 2024](#)) have a limited potential for this purpose, indirect methods like double-peaked emission lines ([L. Blecha et al. 2013](#); [A. Doan et al. 2020](#)), periodicities in optical and radio light curves ([E. Bon et al. 2012](#); [M. J. Graham et al. 2015](#); [S. O'Neill et al. 2022](#)) and cross-symmetric (X, S or Z) radio sources ([X.-G. Zhang et al. 2007](#); [P. Kharb et al. 2017](#); [X. Yang et al. 2022](#)) have been employed to short-list dual AGN candidates.

In spectroscopic surveys using relatively large fibers (e.g., the 3 arcsec diameter fibers used in the Sloan Digital Sky Survey), light from dual AGNs gets integrated/aggregated if the two nuclei are encompassed within the fiber. In that situation, a sufficiently high-resolution optical spectrum may reveal ‘double-peaked’ narrow emission lines (DPNELs), each peak corresponding to the narrow-line region (NLR) of one member of the AGN pair. However, such double-peaked emission lines could also arise from other processes, such as bi-conical outflows of warm gas, bulk rotation of the NLR gas, and jet-cloud interactions ([F. Müller-Sánchez et al. 2015](#); [R. Nevin et al. 2016](#); [K. Rubinur et al. 2019](#)). Taking the double-peaked optical spectra as the starting point, a fairly high frac-

tion (42/140, i.e. $\sim 30\%$) AGN systems have been confirmed, to date, as dual AGN, using spatially-resolved imaging and spectroscopy, near-infrared adaptive optics imaging and double peak narrow emission lines ([H. Fu et al. 2011](#); [R. C. McGurk et al. 2015](#)). In order to further investigate the origin of DPNELs, follow-up observations including high spatial-resolution imaging combined with spatially-resolved spectroscopy are required ([J. Shangguan et al. 2016](#); [H. Fu et al. 2011](#)). Furthermore, only 5% of the 930 DPNEL galaxies ([J.-M. Wang et al. 2009](#); [K. L. Smith et al. 2010](#); [H. Landt et al. 2010](#); [J.-Q. Ge et al. 2012](#)) at $z \leq 0.15$ have thus been followed up with sub-arcsec imaging in optical and near-infrared (NIR) bands. Only about a sixth of such systems with indications of a dual-component structure from sub-arcsecond imaging have been confirmed spectroscopically (see, [P. Severgnini et al. 2021](#)) and references therein). Interestingly, out of the sample of double-peak AGNs, one parsec-scale binary SMBH, namely J0402+379, has robustly been confirmed through the detection of a pair of compact, variable, flat-spectrum, active galactic nuclei in multi-frequency Very Large Baseline Array (VLBA) observations ([R. W. Pfeifle et al. 2024](#), and references therein). All this underscores the potential of DPNEL galaxies as the hosts of a dual/binary BH pair inside the galactic core.

In addition, X-shaped radio morphologies of jets/lobes have long been linked to the presence of binary SMBHs (e.g., [M. C. Begelman et al. 1980](#)) such that gravitational interaction between the two SMBHs can induce jet precession or, ultimately, even jet reorientation (spin-flip) ([H. Rottmann 2002](#); [D. Merritt & R. D. Ekers 2002](#); [J. Dennett-Thorpe et al. 2002](#); [A. Babul et al. 2013](#)) in the aftermath of the SMBH coalescence ([C. Zier & P. L. Biermann 2001](#); [H. Rottmann 2002](#)). For instance, in a multi-frequency VLA observation of XRG J0725+5835, [X. Yang et al. \(2022\)](#) found a double radio core with nonthermal radio emission exhibiting the signature of jet reorientation in 5 GHz high-resolution European VLBI Network observations. Hence we also note that several other physical mechanisms, such as diversion of the synchrotron plasma streaming backwards from the terminal hotspots in the two primary lobes, or jet-shell interaction, have also been invoked to explain the formation of XRGs (see reviews by [Gopal-Krishna et al. \(2012\)](#) and [G. Giri et al. \(2024\)](#) and references therein). [D. Merritt & R. D. Ekers \(2002\)](#) have suggested that many Z- or S-shaped radio sources are associated with binary SMBHs approaching coalescence, whereas at least some of the X-shaped radio sources showing off-axis, oppositely-directed radio protrusions may represent merged SMBH systems post the gravitational radiation stage (see also, [C. Zier & P. L. Biermann 2001](#); [H. Rottmann 2002](#)). In such a merger event, the active SMBH’s spin angular momentum axis would flip, and the re-energized jets would normally go off in a significantly

changed direction. Thus, binary SMBHs, being the progenitors of the coalesced SMBHs, could eventually be successfully used to constrain the SMBH merger rate and the related physics. On the other hand, wing formation, a marker of X-shaped radio morphology could even begin during the pre-coalescence stage, due to the interaction of the jet pair with the circum-galactic medium of the host elliptical galaxy, which has been set in organized rotation by the in-spiraling of the secondary SMBH (hosted by a smaller galaxy) towards the primary SMBH (Gopal-Krishna et al. 2003). From all these considerations, it becomes important to try to find and investigate SMBH binaries, their rarity notwithstanding.

In this article, we examine the scenario of XRGs hosting dual/binary SMBHs, as hinted by the two key indirect indicators, namely the XRG morphology and double-peak narrow emission lines (DPNELs), discounting for the moment the above-mentioned alternative possibilities for the origin of DPNELs. Simultaneously, we shall also probe the role of radio power output of the AGNs in this context. Some related results based on our Very Long Baseline Interferometry (VLBI) of 4 XRGs will also be presented. This paper is structured as follows. Section 2 describes the observations and sample selection. This is followed by the analysis in Section 3 and our results and discussion in Section 4. The conclusions of this study are summarized in Section 5. Throughout, we have assumed a flat Universe with $H_0 = 70 \text{ km s}^{-1} \text{ Mpc}^{-1}$, $\Omega_m = 0.3$, and $\Omega_\Lambda = 0.7$.

2. OBSERVATIONS AND SAMPLE SELECTION

To probe the possible binary black hole scenario for the formation of XRGs, we compiled a list of 763 XRGs from the literature. The sources were selected from several published works, including C. C. Cheung (2007), D. D. Proctor (2011), X. Yang et al. (2019), and S. Bera et al. (2020), primarily drawn from the images obtained in the 1.4 GHz VLA FIRST survey (R. H. Becker et al. 1995). A summary of the sample, including the catalogs used, the sample sizes (after accounting for any common sources among the catalogs), and details of the final XRG sample, is presented in columns 2 and 3 of Table 1.

In particular, the Sample 3 (X. Yang et al. 2019) contains 290 XRGs, comprising 106 classified as ‘strong’ candidates and 184 as ‘probable’ candidates. Both strong and probable candidates have been included in our sample. Additionally, we have included the 123 new XRG from Patra et al. (in preparation), picked out of the LOFAR Two-metre Sky Survey DR2 survey (T. W. Shimwell et al. 2022), resulting in the final sample of 763 XRGs (see Table 1).

2.1. Optical: Spectral

We first searched for the optical spectra in the Sloan Digital Sky Survey (SDSS) DR 18 (A. Almeida et al. 2023) and

Table 1. Samples of XRG candidates from the literature

Source	Sample /Overlap	Final sample	Survey
1. C. C. Cheung (2007)	100/0	100	1.4 GHz VLA ^b
2. D. D. Proctor (2011)	156/21	135	1.4 GHz VLA ^b
3. X. Yang et al. (2019)	290/25 ^a	265	1.4 GHz VLA ^b
4. S. Bera et al. (2020)	161/21	140	1.4 GHz VLA ^b
5. Patra et al. 2025 (to be submitted)	123/0	123	144 MHz LOFAR ^c
Total	830	763	

^aIncludes 106 strong and 184 probable candidates.

^b(R. H. Becker et al. 1995)

^c(T. W. Shimwell et al. 2022)

the Dark Energy Spectroscopy Instrument (DESI) Data Release 1 (D. Collaboration et al. 2025). For 487 of the 763 XRGs, spectra could be found, and these span a redshift range, $0.0054 \leq z \leq 4.25$. We then primarily used the prominent [O III] $\lambda 5007$ nebular emission line to designate a source as a DPNEL galaxy. To characterize the double-peak nature, we estimated the equivalent width of [O III] $\lambda 5007$ emission line, and selected a subset of 275 sources for which the [O III] $\lambda 5007$ equivalent width of $\geq 3 \text{ \AA}$ (see Section 3). Finally, in order to be able to determine the AGN fraction among the selected DPNEL sources, based on the locations of individual sources in the emission-line diagnostic map, a prerequisite was that the [N II] $\lambda 6548, 6584$ and H α emission lines are covered within the SDSS and DESI spectral wavelength ranges of 3600–10400 Å and 3600–9800 Å, respectively. These requirements imposed together limited our XRG samples to $z \leq 0.58$ and $z \leq 0.49$, respectively. Following the afore-mentioned selection criteria, a total of 187 XRGs became available to us for emission-line fitting.

2.2. VLBA observations

To address whether the galaxies exhibiting the X-shaped morphology and double-peaked [O III] $\lambda 5007$ nebular emission line harbor binary SMBH, we have carried out VLBA observations on a small set of four XRGs that exhibit a prominent double-peaked [O III] $\lambda 5007$ nebular emission line. Among the four proposed XRGs, 3C 223.1, TXS1244+200 and J1430+5217 were selected from the XRG catalogs of D. Merritt & R. D. Ekers (2002), X. Yang et al. (2019) and H. Landt et al. (2010), respectively. In addition, we observed a radio galaxy, J2315+1027, with a hint of radio spur as a possible XRG with double-peaked emission lines.

The VLBA 1.5 GHz (L-band) data for these four double-peaked XRGs were acquired using either nine (BJ095A and BJ095D) or ten (BJ095B and BJ095C) antennas of the VLBA in phase-referencing mode, between 08 March 2019 and 03

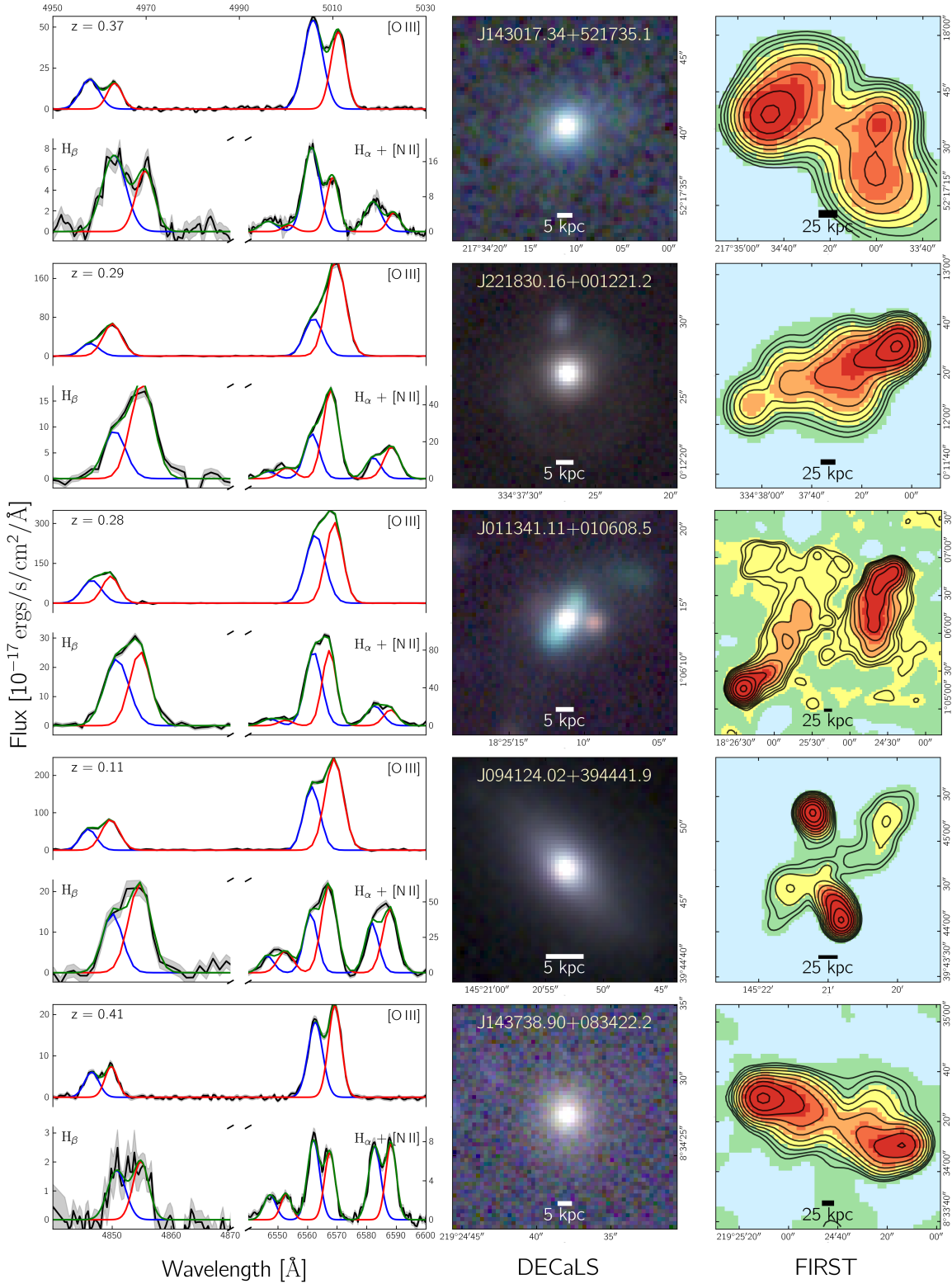


Figure 1. *Left:* Double peak emission line profiles for [O III] $\lambda\lambda 4959, 5007$, $H\beta$, $H\alpha$, and [N II] $\lambda\lambda 6548, 6584$ for five XRGs in the sample. The observed spectra (black) were fitted with Gaussian components, where the blue and red curves represent the blue- and red-ward components, respectively. *Middle:* Color composite (grz) optical images from DECaLS showing the host galaxy morphology. *Right:* Radio continuum contours from the VLA FIRST 1.44 GHz, highlighting the extended radio wings. The scales represent the physical size of the galaxy at the redshift.

June 2019 (Proposal ID: BJ095, PI: Joshi, R.). The observations were conducted with an antenna recording rate of 2 Gbps, using two 128-MHz basebands in both left and right circular polarizations, yielding a total recording bandwidth of 512 MHz. The calibrators 3C 286, OQ 208, 3C 48, and 3C 84 were used as fringe finders and bandpass calibrators. The following combos of target - calibrator were used as phase referencing observations: TXS 1244+200 - J1248+2022; J2315+1027 - J2310+1055; 3C 223.1 - J0934+3926; J1437+5112 - J1430+5217. A standard “nodding” phase-referencing strategy was employed, consisting of 4 minutes on the target source followed by 1 minute on the phase calibrator. The observation information can be found in Table 2.

The observational data from each station were then transferred to the VLBA correlation center in Socorro (New Mexico, USA) for correlation at the Distributed FX (DiFX) correlator (A. T. Deller et al. 2011) with 2s integration time. Then we use the AIPS (Astronomical Image Processing System) software from the US National Radio Astronomy Observatory (NRAO) (E. W. Greisen 2003) to perform data calibration following the standard calibration procedure⁹.

3. ANALYSIS

In this section, we model the spectra to characterize the double-peak [O III] $\lambda 5007$ emission line. At first, we dereddened the SDSS spectra by applying the galactic dust maps with a Milky Way extinction curve from E. L. Fitzpatrick (1999). In order to model the galaxy spectra, we used the publicly available spectral fitting code PYQSOFIT (H. Guo et al. 2018; W. Ren et al. 2024), which uses two independent sets of eigenspectra — pure galaxy and pure quasar — to decompose the spectrum into host galaxy and quasar continuum. The continuum of the host-free spectrum is modelled by a combination of power law, [Fe II], and Balmer continuum models for which the Penalized Pixel-Fitting (pPXF) routine (M. Cappellari 2023) is used to fit the underlying stellar population. In brief, the pPXF masks the emission lines and models the spectrum using simple stellar population templates from MILES (A. Vazdekis et al. 2010), which cover a broad metallicity range (M/H from -2.32 to +0.22) and age ranging between 63 Myr to 17 Gyr.

In order to constrain the double-peak nature of prominent emission lines such as H β , [O III] $\lambda\lambda 4959, 5007$, H α , [N II] $\lambda\lambda 6548, 6584$, and [S II] $\lambda\lambda 6716, 6731$ in the XRG spectra, we followed the emission line classification scheme from J.-Q. Ge et al. (2012). Given that the [O III] $\lambda 5007$ is a prominent nebular emission line and an excellent tracer of the extent and kinematics of diffuse ionized gas, we used it as a

template for model-fitting all other narrow emission lines of interest, i.e., H β , H α , [N II], and [S II]. We thus placed the sources in the four groups, namely: 1) Single peak, 2) Single peak with a broad underlying component, 3) Double peak, and 4) Double peak with a broad underlying component. We did this by modeling all these emission line components simultaneously and estimated the fitted parameters and their rms uncertainties using a non-linear optimization routine ‘LMFIT’ (M. Newville et al. 2024).

We simultaneously fit the [O III] $\lambda 5007$ emission line using single and double narrow Gaussian profiles, with a typical line width of $\lesssim 500 \text{ km s}^{-1}$. Following J.-Q. Ge et al. (2012) and D. Maschmann et al. (2020), we deem a source double-peaked only if it satisfies the following 3 criteria:

1. The ratio of amplitudes of the two [O III] components is between 1/2.5 and 2.5. This would more likely ensure a clear identification of two peaks and avoid the false positives due to a weak outflow/inflow component.
2. Both the peaks are well separated by at least 3 times the spectral resolution offered by the SDSS (i.e., $\sim 210 \text{ km s}^{-1}$) and DESI (i.e., $\sim 120 \text{ km s}^{-1}$).
3. The F-test demonstrates that incorporating the double-peaked profile, as the case may be, yields a significantly better fit compared to the single-peaked model, with a significance level of 5%. We further verified this by ensuring a lower Bayesian Information Criterion (BIC) value (G. Schwarz 1978; A. R. Liddle 2007) for the double-peaked profile as compared to the single-peaked one.

An underlying broad-line component was required by the fitting process in the case of just 27 XRGs; however, we have not assigned any physical significance to it. Among the 187 of the XRGs subjected to [O III] $\lambda 5007$ line fitting, we classified 55 as having double-peaked emission line profiles. Subsequently, we used the [O III] $\lambda 5007$ model as a template to fit the other prominent narrow emission lines like H β , [O III] $\lambda 4959$, [N II] $\lambda\lambda 6548, 6584$, H α , and [S II] $\lambda\lambda 6716, 6731$. The widths and redshift (velocity offset) of the different Gaussian components were tied to the corresponding [O III] $\lambda\lambda 4959, 5007$ line components. Additionally, we set the flux ratios of [O III] $\lambda 5007$ /[O III] $\lambda 4959$ at 3.00 and [N II] $\lambda 6584$ /[N II] $\lambda 6548$ at 2.96 (D. E. Osterbrock & G. J. Ferland 2006). Since the broad component is deemed to hold no physical significance, we kept its width as a free parameter for all emission lines to achieve χ^2 improvement by 20%, wherever necessary.

⁹ see Appendix C of AIPS Cookbook in <http://www.aips.nrao.edu/cook.html>

Table 2. The VLBA observations

Code	Date	Target: XRG	Phase Calibrator	Time	Telescopes ^a
	(YYYY/MM/DD)	(J2000)	(J2000)	(h)	
bj095a	2019/04/27	TXS 1244+200	J1248+2022	10.4	BR,FD,HN,KP,LA,MK,NL,OV,PT
bj095b	2019/03/08	J2315+1027	J2310+1055	5.2	BR,FD,HN,KP,LA,MK,NL,OV,PT,SC
bj095c	2019/03/13	3C 223.1	J0934+3926	5.2	BR,FD,HN,KP,LA,MK,NL,OV,PT,SC
bj095d	2019/03/22	J1430+5217	J1437+5112	5.2	BR,FD,HN,LA,MK,NL,OV,PT,SC

Note: Col. 1 - Observation code of VLBA sessions; Col. 2 - Observation date; Col. 3 - The target of the observation session; Col. 4 - Phase calibrator of the phase referencing session; Col.5 - Overall observing time of the session; Col. 6 - Telescopes participating in the VLBA observation.

^aVLBA telescopes participating in the observations: BR (Brewster), FD (Fort Davis), HN (Hancock), KP (Kitt Peak), LA (Los Alamos), MK (Mauna Kea), NL (North Liberty), OV (Owens Valley), PT (Pie Town), SC (Saint Croix).

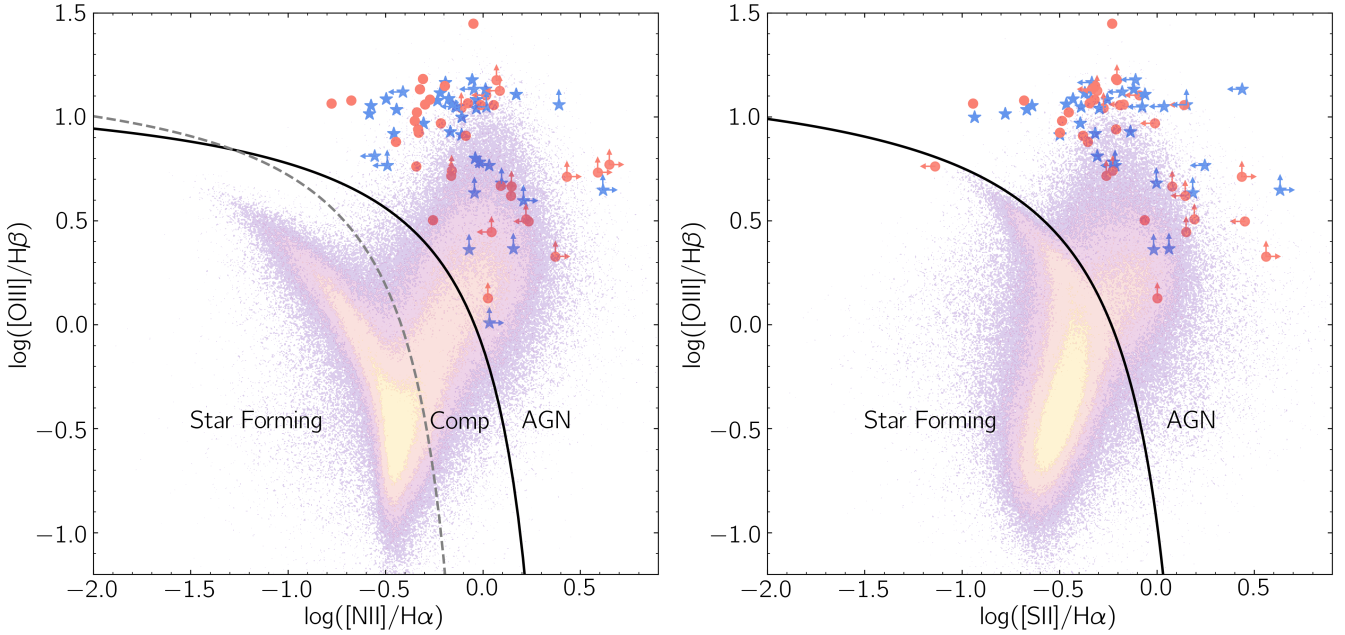


Figure 2. *Left Panel:* The [N II]-BPT diagnostic map for the double-peaked XRGs. The line ratios for the blue and red emission line components are shown as *circle* and *stars*, respectively. The upper and lower limits are marked with an arrow. The *dashed* and *solid* line demarcates the AGN from star-forming galaxies based on the BPT classification from G. Kauffmann et al. (2003) and L. J. Kewley et al. (2006), respectively. The region between the two lines is demarcated as *Comp*, which stands for composite, indicating photoionization from both star-forming regions and AGN. *Right:* Same as left panel for [S II]-BPT diagnostic. The colored shaded region in both panels depicts the BPT density map from the SDSS DR8 value added catalog (H. Aihara et al. 2011).

4. RESULTS AND DISCUSSION

4.1. Occurrence of dual-AGN candidates in XRGs

To estimate the fraction of dual-AGN within DPNEL XRGs, we use the Baldwin, Phillips & Terlevich (BPT) diagnostic diagrams, which provide an empirical classification using various emission-line ratios, in order to effectively differentiate between photoionization produced by the harder AGN spectrum (i.e., a larger fraction of higher energy photons) and that produced by hot stars (J. A. Baldwin et al. 1981). In Figure 2, we show the BPT-diagram based on [N II] λ 6584/H α versus [O III] λ 5007/H β and [S II] λ 6716,6731/H α versus [O III] λ 5007/H β line ratios. The

extreme starburst line for pure stellar photoionization models by G. Kauffmann et al. (2003) is shown as a *solid line* whereas the modified model for dividing the pure star-forming galaxies from AGN and H II composite sources by L. J. Kewley et al. (2001) is shown as a *dashed line*. We note that, for 3 of our sources, the H α spectral line region is either corrupted or lies near the edge of the spectral range covered, reducing the sample to 52 XRGs available for BPT analysis. We detected all the nebular emission lines available, i.e., H α , H β , [N II] λ 6548, at $\geq 3\sigma$ level only for 16 XRGs out of the 52 DPNELs. The line ratios for the blue and red components are shown as *stars* and *circles*, respectively. However, we could only obtain upper or lower limits on line ratios for

the cases where any of the lines is detected at $< 3\sigma$ level and this is the case for 21 XRGs (see Figure 2). It is important to note that 33 out of 37 XRGs ($\sim 90\%$) present in the [NII] BPT diagram reside within the locus where the emission lines are primarily excited by the AGN activity. These estimates of fractions include the possibility that the individual data points for which only upper/lower limits are available can accordingly move across the respective diagrams. Similarly, in the [SII] BPT diagram, available for 48 out of 52 XRGs, we detect 13 galaxies where all emission lines are present at $\geq 3\sigma$, while upper and lower limits can be determined for the remaining 21 sources. It shows that $\sim 85\%$ (29/34) of these XRGs lie within the AGN domain. Taking both the diagnostics, we find that 35/37 ($\sim 95\%$) XRGs are dual AGN.

Here, it is interesting to recall that for the general galaxy population, the fraction of galaxies hosting DPNELs is found to be merely $\sim 1\%$ and only $\sim 30\%$ of these are cases where both line components are classified as AGN, hence dual-AGN candidates (J.-Q. Ge et al. 2012; D. Maschmann et al. 2020). In contrast, for the XRGs, we find the fraction of DPNELs to be at least 30% (55/187) and, moreover, $\sim 95\%$ are found to be of dual-AGN type. This immediately begs the question about the origin of the huge jump in the dual-AGN candidate fraction from $\sim 0.3\%$ for the general galaxy population to $> 30\%$ found here for XRGs. Is this 2 orders-of-magnitude jump linked to the XRG morphology, or more generally, to the difference in radio luminosity? To enquire this, we now extend the present analysis to encompass classical double radio sources of Fanaroff-Riley type II (B. L. Fanaroff & J. M. Riley 1974).

4.2. Occurrence of dual-AGN candidates at different radio luminosities

The above analysis has already provided the occurrence rates of dual-AGN candidates among the general galaxy population and for the XRG population. Given the prevalence of overwhelming dual AGN signatures in DPNEL XRGs, it is worth exploring the AGN fraction in DPNEL FR-II radio galaxies whose radio powers can be comparable to or even exceed those of the XRGs. For this, we employ the FR-II radio source catalog from B.-Q. Lao et al. (2024), comprising 45,241 FR II galaxies. It spans a wide range of luminosities $2.63 \times 10^{22} \leq L_{\text{rad}}^{1.4\text{GHz}} \leq 6.76 \times 10^{29} \text{ W Hz}^{-1}$ and redshift $0.0 \leq z \leq 5.01$. We further searched for the optical spectra in SDSS and DESI datasets, following the selection criteria outlined in Sec: 2.1, resulting in 199 sources with [OIII] $\lambda 5007$ emission line equivalent width of $\geq 3 \text{ \AA}$. By employing the multiple emission line modelling, explained in Sec-3, we found 21 ($\sim 10\%$) FR-II sources to have double-peaked emission lines. For 16 sources with the corresponding line ratios determined within limits, the BPT line diag-

nostic classified all but one as dual AGN, yielding a $\sim 94\%$ dual AGN candidate fraction in FR-II radio galaxies.

In order to examine the radio luminosity dependence of the dual AGN fraction in DPNEL galaxies, we matched the 3030 DPNEL galaxies from J.-Q. Ge et al. (2012) against the 1.4 GHz FIRST catalog (R. H. Becker et al. 1995), resulting in a subsample of 431 radio-detected galaxies. In Figure 3, we compare these dual AGN fractions in radio-detected galaxies, which include both the XRGs and FR-II sources. It is evident that the dual AGN fraction strongly correlates with the radio luminosities. While among the radio-detected DPNEL galaxies, overall $\sim 58\%$ of the radio-detected galaxies are classified as dual AGN, whereas the fraction crosses 94% for the XRGs and FR-II radio galaxies. Interestingly, the dual AGN fraction drops to 25% in the case of radio-undetected DPNEL galaxies (see Fig: 3).

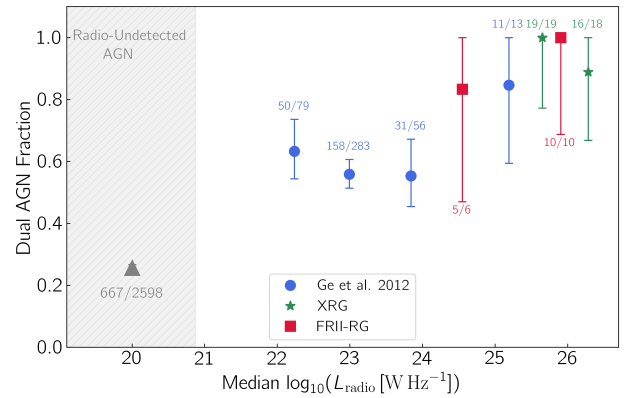


Figure 3. The radio luminosity dependence of dual AGN fraction in double-peaked emission line galaxies based on BPT diagnostics. The radio-undetected and radio-detected DPNEL galaxies from J.-Q. Ge et al. (2012) are shown as triangles and circles, respectively. The errors correspond to 1σ confidence level and are computed using the standard Poisson statistics N. Gehrels (1986). The higher fraction of dual AGNs in XRGs (stars) and FR-II radio galaxies (squares) underscores the radio dependence.

4.3. XRGs with double-peak spectrum versus the normal XRGs

Here, we compare the physical properties of XRGs with and without DPNELs, along with FRI and FR-II-type radio galaxies. Recall that the mass of the central SMBHs is found to be tightly correlated with the stellar mass of the bulge of the host galaxy (J. Kormendy & L. C. Ho 2013). We determine the SMBH mass based on the galaxy stellar mass versus black hole mass scaling relation from J. E. Greene et al. (2020, see below) for 187 XRGs, including 55 XRGs with DPNEL. For 141 XRGs with SDSS spectra, we obtained the multi-band optical (u, g, r, i, z) photometry data from the SDSS DR16 survey (R. Ahumada et al. 2020), comple-

Table 3. Summary of the model parameters for [O III] $\lambda 5007$ nebular emission, including flux, velocity dispersion and relative redshift of the individual components (z), along with derived properties such as black hole mass, potential separation, NLR radii, and redshifts for 10 out of 55 XRGs exhibiting DPNELs[‡]. The final column, T , denotes the BPT classification: $T = 1$ indicates that both components are classified as AGN, $T = 0$ corresponds to cases where multiple robust lines are not detected and hence no classification is possible, and $T = 2$ represents all other cases, such as AGN + star forming (SF) or SF+SF.

SDSS Name J2000	z	$\log M_{\text{BH}}$ [M_{\odot}]	$\log R_{\text{NLR},1}$ [pc]	$\log R_{\text{NLR},2}$ [pc]	$F_{[\text{O III}] 5008}$ [erg s ⁻¹ cm ⁻²]		$\sigma_{[\text{O III}]}$ [km/s]		$z_{1,2}$		T
					n1	n2	σ_1	σ_2	z_1	z_2	
J011341.11+010608.5	0.2809	8.6 ± 0.10	3.9 ± 0.03	3.9 ± 0.03	1178.96 ± 11.88	1191.05 ± 11.42	126.3 ± 2.4	108.2 ± 1.6	0.2805	0.2813	1
J014316.72-011901.0	0.5193	8.6 ± 0.10	3.8 ± 0.03	3.7 ± 0.03	35.87 ± 4.76	31.37 ± 4.74	132.0 ± 30.5	183.6 ± 79.3	0.5189	0.5199	0
J014719.28-085119.6	0.4547	7.9 ± 0.12	3.7 ± 0.03	3.9 ± 0.03	342.99 ± 2.92	128.8 ± 4.2	115.1 ± 2.2	189.2 ± 2.8	0.4532	0.4550	1
J021635.79+024400.9	0.1451	9.3 ± 0.13	3.3 ± 0.04	3.5 ± 0.04	37.81 ± 6.31	139.85 ± 13.45	≥ 42.0	≤ 198.0	0.1445	0.1450	0
J065514.73+540857.2	0.2380	9.5 ± 0.13	3.9 ± 0.03	4.1 ± 0.04	809.42 ± 10.68	4493.35 ± 14.73	68.8 ± 2.5	190.1 ± 1.3	0.2375	0.2382	1
J072423.22+362032.2	0.2970	9.0 ± 0.11	3.5 ± 0.03	3.6 ± 0.03	44.45 ± 4.78	68.03 ± 5.81	92.9 ± 16.6	109.7 ± 16.4	0.2965	0.2974	1
J072645.57+510407.0	0.3390	10.2 ± 0.18	4.0 ± 0.03	3.9 ± 0.03	1011.98 ± 8.05	464.51 ± 6.36	190.2 ± 7.7	92.3 ± 4.4	0.3385	0.3393	1
J074125.22+333319.9	0.3640	8.7 ± 0.10	4.2 ± 0.05	4.1 ± 0.04	1202.66 ± 9.48	124.57 ± 5.02	194.7 ± 5.0	72.8 ± 8.3	0.3634	0.3652	1
J074845.10+232445.8	0.1901	9.0 ± 0.11	3.5 ± 0.03	3.4 ± 0.04	93.91 ± 6.13	46.02 ± 5.24	85.0 ± 12.8	61.6 ± 11.6	0.1899	0.1905	1
J081841.57+150833.5	0.3304	8.9 ± 0.11	3.9 ± 0.03	3.6 ± 0.03	425.70 ± 6.68	87.32 ± 4.82	≤ 170.3	≤ 96.3	0.3299	0.3310	1

[‡] The table for remaining sources and fitted flux for other emission lines is provided in a machine-readable format.

mented by mid-infrared (3.4 and 4.6 μm ; W1 and W2 bands) data from the unWISE catalog (E. F. Schlafly et al. 2019). Next, we model the spectral energy distribution (SED) of XRGs using the piXedfit routine, which uses a Bayesian technique to estimate the underlying parameters (Abdurro'uf et al. 2021). For this, we used the model with a wide parameter space, including double power-law star formation history (A. C. Carnall et al. 2018), initial mass function (G. Chabrier 2003), dust attenuation ($0 \leq A_v \leq 3$) (S. Charlot & S. M. Fall 2000), and dust emission (B. T. Draine & A. Li 2007). Further, to account for the contribution from the active black hole, we added the emission from the dust torus heated by the AGN (M. Nenkova et al. 2008a,b). In addition, for 46 DESI XRGs, we use the stellar mass estimates provided by the DESI value-added catalog (M. Siudek et al. 2024), where the SED modelling is performed with a similar parameter space using DESI g , r , z and W1 and W2 bands. For all but 3 XRGs with the best fit SED, the stellar masses range from $10^{9.83} M_{\odot}$ to $10^{12.46} M_{\odot}$ with a median of $10^{10.86} M_{\odot}$. Using the $M_{\text{BH}} - M_*$ scaling relation by J. E. Greene et al. (2020, see their early-type galaxies in their Table 9), we estimate the black hole mass as:

$$\log M_{\text{BH}} = (7.89 \pm 0.09) + (1.33 \pm 0.12) \log \left(\frac{M_*}{3 \times 10^{10} M_{\odot}} \right) + (0.65 \pm 0.05). \quad (1)$$

The estimated black hole masses for XRGs with DPNELs are presented in column 2 of Table 3. In the upper panel of Figure 4, we compare the SMBH mass distributions of XRGs with and without DPNELs.

The black hole masses for XRGs with DPNEL range from $7.71 \leq \log M_{\text{BH}} [M_{\odot}] \leq 11.05$, with a median of

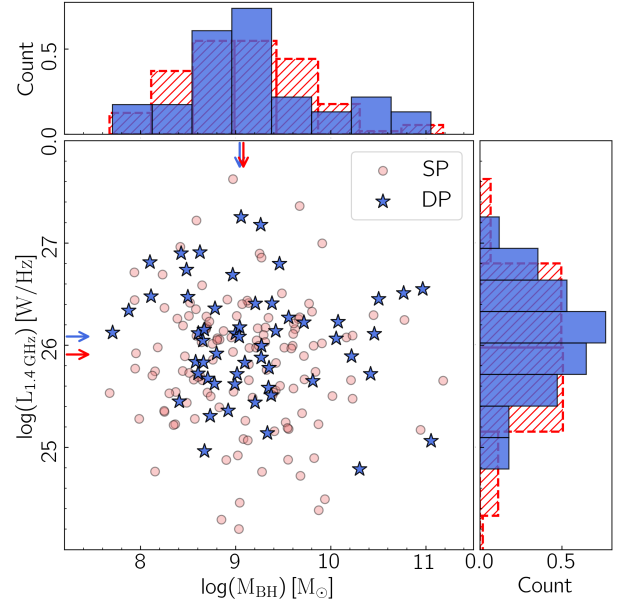


Figure 4. The black hole mass versus 1.4 GHz radio luminosity for the single-peaked (circle) and double-peaked (stars) XRGs. The double-peaked XRGs ($\langle \log M_{\text{BH}} \rangle = 9.04 \pm 0.11 M_{\odot}$) host very similar black hole masses as compared to single-peaked XRGs ($\langle \log M_{\text{BH}} \rangle = 9.08 \pm 0.12 M_{\odot}$). The radio luminosities of double-peaked XRGs ($\langle \log L_{1.4 \text{ GHz}} \rangle = 26.08 \pm 0.01 \text{ W Hz}^{-1}$) are also similar to those of single-peaked XRGs ($\langle \log L_{1.4 \text{ GHz}} \rangle = 25.91 \pm 0.02 \text{ W Hz}^{-1}$).

$\langle \log M_{\text{BH}} [M_{\odot}] \rangle = 9.04 \pm 0.11$. In addition, XRGs without double peak emission lines exhibit a similar average black hole mass of $\langle \log M_{\text{BH}} [M_{\odot}] \rangle = 9.08 \pm 0.12$, ranging from $7.67 \leq \log M_{\odot} [M_{\odot}] \leq 11.18$. A Kolmogorov–Smirnov (KS) test yields a null probability value of $p_{\text{null}} = 0.58$, sup-

porting the null hypothesis that the SMBH mass distributions of XRGs with and without DPNELs are drawn from the same parent population. This hints that XRGs with and without double-peaked emission lines have gone through a similar evolutionary phase. All the DPNEL XRGs showing two active AGNs in a BPT diagram highlight that the XRGs are probably commonly formed through a merger. Thus, the similar black hole masses in XRGs with and without DPNEL can be reconciled under a common evolutionary phase. A larger sample of double-peak XRGs taken from next-generation optical and radio surveys should help to understand this further.

In previous efforts to constrain the formation scenarios of XRGs, involving either the merger of two SMBHs leading to the jet reorientation or the presence of two active SMBHs, [M. Mezcuca et al. \(2011\)](#) analyzed 29 XRGs from a sample of 100 sources selected by [C. C. Cheung \(2007\)](#). They found that the XRGs are hosted in elliptical galaxies, likely formed through hierarchical mergers (see also, [G. Efstathiou & J. Silk 1983](#); [C. S. Frenk et al. 1988](#); [P. F. Hopkins et al. 2006b](#)). Additionally, the average black hole mass in XRGs ($\langle \log M_{\text{BH}} [M_{\odot}] \rangle = 8.32$) was found to be 1.94 times higher than that of a limited control sample of 20 radio galaxies, including 10 each of elliptical and FR II radio galaxies, with similar redshifts and comparable optical and radio luminosities, i.e., $\langle \log M_{\text{BH}} [M_{\odot}] \rangle = 8.04$. However, using a larger set of 106 XRGs, [R. Joshi et al. \(2019\)](#) have found the average black hole mass of XRGs ($\langle \log M_{\text{BH}} [M_{\odot}] \rangle = 8.81$) to be slightly lower than that of a control sample of 388 FR II radio sources hosting powerful jets ($\langle \log M_{\text{BH}} \rangle = 9.07 [M_{\odot}]$). The relatively lower black hole mass of XRGs compared to their more powerful FR II counterparts suggests that even minor mergers can cause jet reorientation, contributing to their distinctive X-shaped radio morphology.

In Figure 4, we compare the black hole mass versus the radio luminosity of XRGs with (*star*) and without (*circle*) double peaks. For this, we estimate the radio flux using the 1.4 GHz NRAO VLA Sky Survey (NVSS), made with a much larger beam of 45'' diameter. The NVSS survey, with good UV spacing, is known to be sensitive to diffuse radio emission of extent up to at least 10 arcmin ([J. J. Condon et al. 1998](#)). Assuming a spectral index of $\alpha \sim -0.7$, we estimate the radio luminosity for all of the XRGs. The radio luminosity for XRGs with DPNEL range from $24.79 \leq \log L_{1.4 \text{ GHz}} [\text{W/Hz}] \leq 27.25$, with an average of $\langle \log L_{1.4 \text{ GHz}} \rangle = 26.08 \text{ W Hz}^{-1}$. We also see that XRGs without DPNEL show similar radio luminosities, ranging from $21.04 \leq \log L_{1.4 \text{ GHz}} [\text{W/Hz}] \leq 27.62$ with average luminosity of $\langle \log L_{1.4 \text{ GHz}} \rangle = 25.91 \text{ W Hz}^{-1}$, hinting that the sources are powered similarly. This aligns with the findings of [X. Yang et al. \(2019\)](#) that XRGs have intermediate radio luminosity between FR II and FR I radio sources. Furthermore, we find that the black hole mass may correlated mildly with ra-

dio luminosity with a Spearman's rank correlation coefficient of $r_s = -0.061$ and a null probability, $p_{\text{null}} = 0.41$.

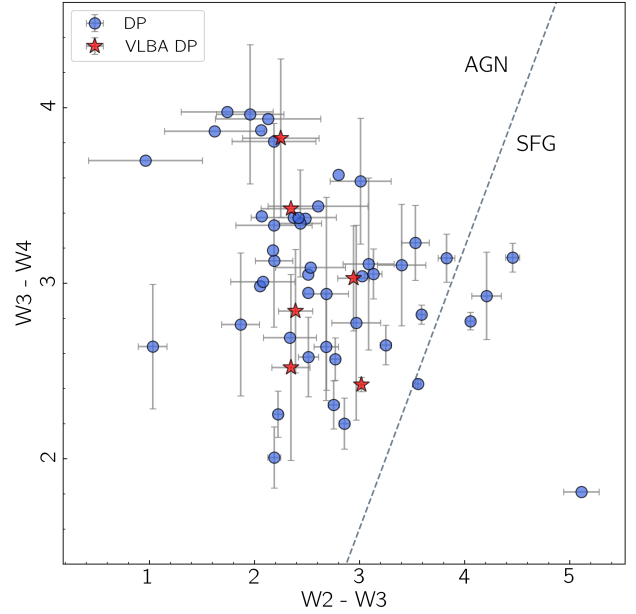


Figure 5. The mid-infrared color diagnostic diagram for the XRGs hosting DPNELs (*circle*) with emphasis on the VLBA sample (*star*). The dotted line ([R. Coziol et al. 2015](#)) separates the AGN locus from the star-forming region. All but 5 (91%) indicate AGN photoionization in agreement with the BPT diagrams (Figure 2).

Finally, we explore the mid-infrared (MIR) color properties of the double-peaked XRGs. The MIR diagnostic colors can be used to distinguish star-forming galaxies from AGNs even in cases where one or both of the AGNs are obscured ([M. Lacy et al. 2004](#); [D. Stern et al. 2005](#); [R. Coziol et al. 2015](#)). Among the 55 XRGs harboring DPNELs, we could obtain the colors of 54 XRGs using four mid-infrared bands of the Wide-field Infrared Survey Explorer (WISE) survey ([E. L. Wright et al. 2010](#)) W1 ($3.4 \mu\text{m}$), W2 ($4.6 \mu\text{m}$), W3 ($12 \mu\text{m}$), and W4 ($22 \mu\text{m}$) in Vega magnitudes. Using the $W3 - W4$ vs $W2 - W3$ classification (see Section 3.1 of [R. Coziol et al. 2015](#)), we find 49/54 (91%) of the sources are ionized by AGNs, which aligns with the similarly high fraction determined from the BPT diagrams.

4.4. Parsec-scale view of XRGs

We now present in Figure 5 the 1.4 GHz VLBA maps from our VLBA campaign of four XRGs exhibiting double-peak emission lines. We also searched the 55 double-peaked XRGs in the "Radio Fundamental Catalogue" ([L. Y. Petrov & Y. Y. Kovalev 2025](#)), which includes all the sources observed with VLBA for absolute astrometry and geodesy from April 11, 1980, to September 5, 2024. As a result, we identified three additional sources with VLBA maps, J1115+4314,

Table 4. VLBA observation log for the dual AGN candidates

Source	Obs Date	ν_{cen} (GHz)	Beam (mas)	Separation (pc)	PA (deg)	RMS (mJy)	z	Spectral Index
3C 223.1	2019-03-13	1.55	10.10×4.34	20	-0.74	0.02	0.11	0.25
	2018-08-11 ^a	4.98	3.46×1.62	6.7	15.56	0.02		0.32 ^{α}
J1115+4314 [‡]	2016-08-14	4.34	4.73×1.89	29	37.4	0.07	0.46	0.54 ^{β}
	2016-08-14	7.62	2.90×1.07	18	39.88	0.09		
J1134+3835 [‡]	2016-08-19	4.34	5.11×4.34	30	36.73	0.08	0.50	0.23
	2016-08-19	7.62	3.05×1.30	18	6.84	0.09		
TXS 244+200	2019-04-27	1.55	16.01×5.70	82	-15.80	0.01	0.43	0.24
J1430+5217	2019-03-22	1.55	9.79×3.78	61	-4.70	0.02	0.37	0.00
	2022-05-25	4.35	5.89×3.4	30	32.8	0.10		0.19 ^{γ}
	2022-05-25	7.62	7.66×2.27	39	87.12	0.20		
J1604+3221 [†]	2014-01-27	4.34	4.61×2.03	27	21.40	0.09	0.45	0.01 ^{δ}
	2014-01-27	7.62	2.65×1.25	15	22.007	0.10		
J2315+1027	2019-03-08	1.55	11.80×4.69	42	-4.72	0.02	0.26	0.49

[‡]S. Bera et al. (2020)[†]Patra et al. 2025 *to be submitted*^aB. Sebastian et al. (2024) ^{α} non-simultaneous spectral index between 1.55 GHz (2019-03-13) and 4.98 GHz (2018-08-11) ^{β} between 4.34 GHz and 7.62 GHz on 2016-08-14 ^{γ} between 4.34 GHz and 7.62 GHz on 2022-05-25 ^{δ} between 4.34 GHz and 7.62 GHz on 2014-01-27

J1134+3835, and J1604+3221, which are reproduced in Fig. 6. We also found additional observations for J1430+5217 at 4.4 GHz and 7.6 GHz. The sample summary, including source name, date of observation, frequency, beam size, root mean squared (rms) noise, redshift, beam size, separation between the optical and radio cores, and in-band spectral index (or dual-band in 'Spectral Index' column), is listed in Table 4.

Among the 7 XRGs, we detect a resolved central parsec core for only one, J2315+1027, in our 1.4 GHz VLBA maps (see Figure 6). At $z = 0.255$, the beam size of 10.4 milliarcsec (mas) offers a spatial resolution of 40 pc. Interestingly, the resolved cores are seen at a separation of ~ 40 pc. (see Fig. 6). At parsec scales, the core is found to extend at a position angle (PA) of 61° , measured from north to east direction. It aligns with the primary kiloparsec-scale jet observed at a PA of 61.2° in the VLA FIRST observations. A follow-up high-frequency VLBA observation constraining the spectral index would help to verify the possibility of a binary black hole or core-jet system. Interestingly, the kpc-scale active FR II-jet is aligned towards the major axis of the optical host galaxy [$z_{\text{spec}} = 0.255$]. This is in agreement with the observed tendency of active jets in XRGs to align along the major axis of their optical host galaxies (R. Joshi et al. 2017). Further, the DECaLS optical field reveals three close companion galaxies with photometric redshifts near that of the XRG, suggesting a potential merger history (see Figure 6).

Another XRG in our sample, 3C 223.1, is known to have a kpc-scale “double-boomerang” morphology. Recently (Gopal Krishna & P. Dabhade 2022) have shown that the wings anomalously exhibit a flatter radio spectrum even compared to the hotspots in the primary lobes, which supports the particle acceleration associated with the rebounding of collimated backflow of synchrotron plasma streaming through the primary lobes. Our 1.4 GHz VLBA maps show a hint of a resolved structure directed toward the currently active radio jets. The resolved jet structure is further supported by the 5 GHz VLBA maps by B. Sebastian et al. (2024, see their figure 4) showing an extended pc-scale morphology, likely indicating a core jet structure. Furthermore, a relatively flat spectral index of $\alpha = 0.32$, derived from the 1.4 GHz and 5 GHz VLBA maps, in conjunction with the presence of double-peaked emission lines in the BPT diagram, suggests that this source is a promising candidate for follow-up study in search of binary AGN.

For the remaining five sources, the core is unresolved, with a typical spatial beam size resolution ranging between 8.7 to 82 pc. Based on multi-frequency VLBA observations available for these 5 sources, we estimate the spectral indices, ranging between 0.01 and 0.54 (see Table 4, column 9). This suggests that in case XRGs with DPNELs host binary SMBHs, their separation must be smaller than the beam size.

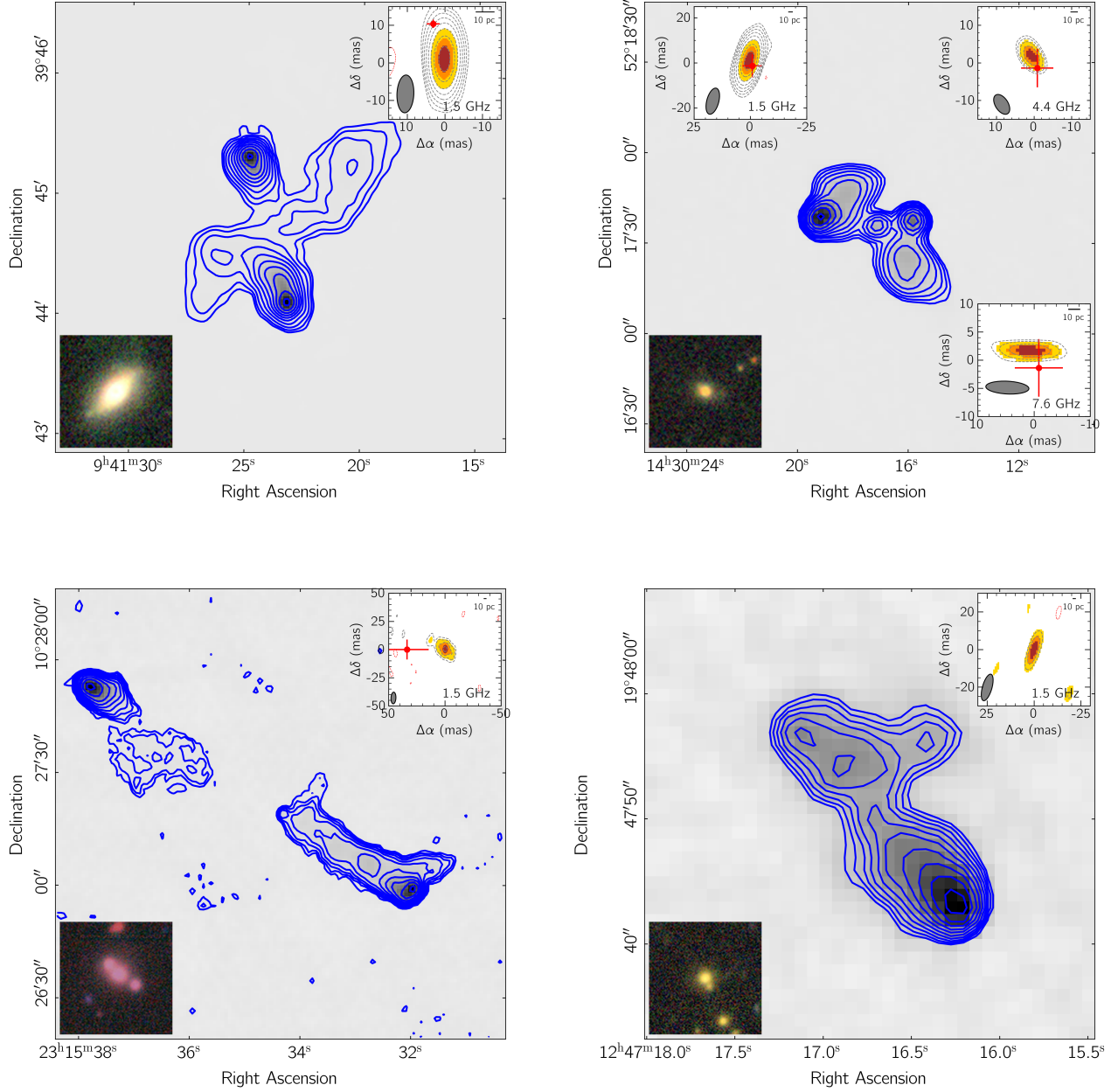


Figure 6. The extended kpc scale radio morphology for 3C 223.1 using 144 MHz LOFAR (*top left*), and maps from the 2.5 GHz VLASS survey for J1430+5217 (*top right*), J2315+1027 (*bottom left*) and TXS 1244+200 (*bottom right*) respectively. The insets show the parsec scale VLBA radio core in available 1.5 GHz, 4.3 GHz, or 7.6 GHz maps and respective beam FWHM. The Gaia DR3 positions are indicated by red crosses, with their lengths representing the 1σ rms errors. The bottom left inset image displays a DECaLS (g, r, z) color composite image of the radio host galaxy.

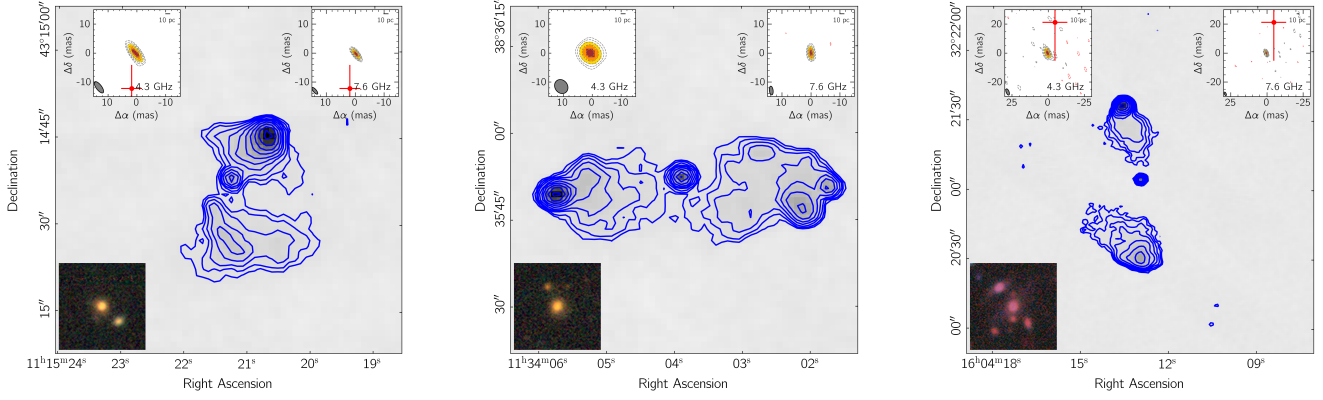


Figure 7. As in Figure 6 with 2.5 GHz VLASS maps showing extended kpc scale radio morphology for J1115+4314, J1134+3835 and J1604+3221 (left to right).

We may recall that the positional offset of radio-optical emission cores may signify the presence of multiple AGNs (Y.-C. Chen et al. 2023; P. Cigan et al. 2024; W. Xu et al. 2024). To test the multi-AGN hypothesis, which we have seen is hinted by multiple indirect indicators, notably DP-NEL, X-shaped morphology, and flat-spectrum core, we compare the spatial positions of VLBA radio maps with those from Gaia DR3 (Gaia Collaboration et al. 2023). We obtain a significant offset (between 1.5 to 33 mas) for 5 out of 7 sources. A flat-spectrum core along with a radio-optical offset in XRGs J1430+5217, J1115+4314, and J1604+3221, makes them strong binary black hole candidates (G. Orosz & S. Frey 2013). Even though a significant offset is detected in 3C 223.1 and J2315+1027 multifrequency observations, the determination of their spectral indices are required to confirm the possibility of dual AGN. For the above sources, the Gaia optical counterparts are offset towards the resolved VLBI components. Such offsets can plausibly arise from a radio-loud core with optical emission rendered undetected (due to obscuration) and a radio-quiet secondary core dominating the emission detected by Gaia. The majority of recent Gaia–VLBI studies at mas or sub-mas level show an offset that could arise from strong optical jet emission preferentially being located either downstream or upstream of the peak of the AGNs jet radio emission (Y. Y. Kovalev et al. 2017; A. V. Plavin et al. 2019). Therefore, other explanations, such as a single core driving both optical and radio emission with significant separation or a frequency-dependent core position shifting due to flaring, cannot be discounted (K. V. Sokolovsky et al. 2011; A. V. Plavin et al. 2019).

We further test the binary black hole scenario, where the DPNELs are taken to have originated from the separate narrow line regions (NLR) of the individual SMBHs. Following

(X. Liu et al. 2013), we determine the size of the NLR as:

$$\log \left(\frac{R_{\text{NLR}}}{\text{pc}} \right) = (0.250 \pm 0.018) \times \log \left(\frac{L_{[\text{O III}]}}{10^{42} \text{ ergs s}^{-1}} \right) + (3.746 \pm 0.028) \quad (2)$$

where $L_{[\text{O III}]}$ represents the $[\text{O III}]\lambda 5007$ luminosity, corrected for the Balmer extinction of the individual emission line components. In the above scenario, one expects the separation of individual NLRs to be smaller than the BH separation. The size of NLR is listed in columns (6) and (7) of Table 3. The NLR size for DPNEL XRGs ranges between 1.52 to 17.74 kpc, which is significantly larger than the expected binary black hole separation of 0.1 kpc (see also C. Villforth & F. Hamann (2015)). Nonetheless, considering the extended structure of the NLR along with the multiple double-peak emission lines ($\text{H}\beta$, and $\text{H}\alpha$) originating in the BLR near the SMBH, the observed DPNEL in the XRGs could still be associated with the binary black hole system (D. Xu & S. Komossa 2009; S. Tang & J. Grindlay 2009). It is worth reiterating that the DPNELs can also arise from alternative processes, notably complex kinematics within the NLR, such as rotating disks and biconical outflows (see Section 1). Follow-up narrow-band imaging and IFS observations would help to distinguish the various possibilities.

The presence of parsec-scale binary SMBHs is further supported by the detection of two compact non-thermal radio cores in high-resolution 5 GHz VLBI observations of the XRG J0725+5835 (X. Yang et al. 2022). In conjunction with the archival VLA 1.5 and 3 GHz data, the radio spectral index map suggests that XRG J0725+5835 corresponds to a dual jetted AGN system extending over 100 kpc. This source shows hybrid morphology with one AGN being a Fanaroff-Riley type I (FR I) source and the other classified as type FR II (Gopal-Krishna & P. J. Wiita (2000)). In addition, they observed lateral flow signatures in the spectral index map of the southern hotspot, providing evidence that the jet from core

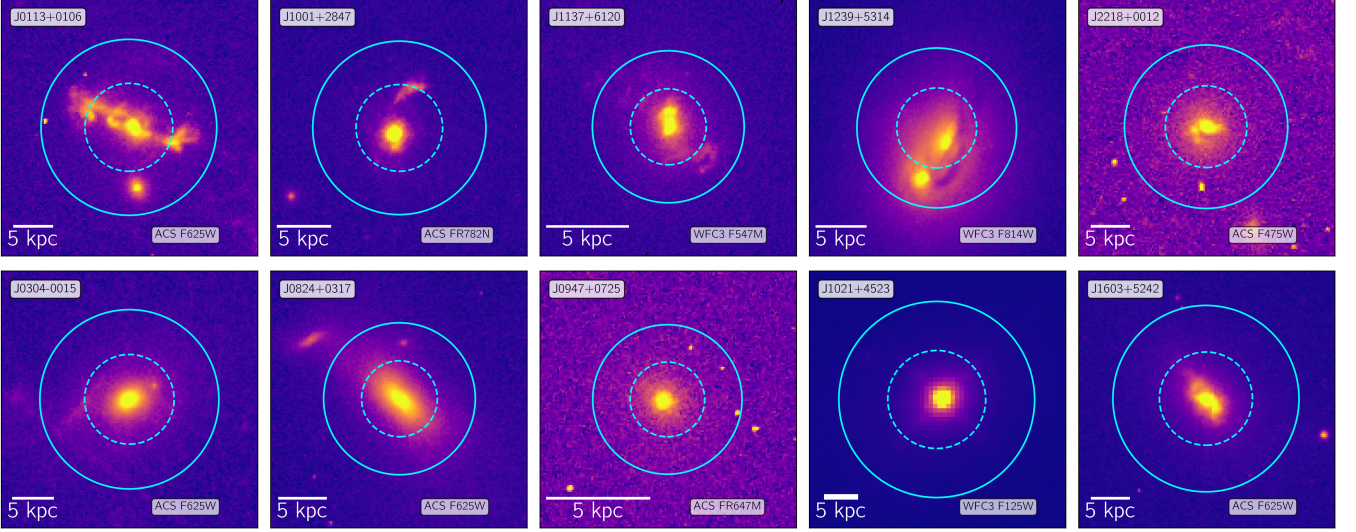


Figure 8. The high-resolution HST/WFC3 images of XRGs with (top panel) DPNELs revealing signatures of galaxy mergers and distinct tidal tails, indicative of an ongoing or recent galactic merger. *Bottom Panel:* HST/WFC3 images of XRGs without DPNELs, showing predominantly isolated host galaxies with no nearby companions, consistent with a post-merger origin. The SDSS and DESI fiber of 3 arcsec *blue circle* and 1.5 arcsec *blue dashed circle* diameter, and DESI fiber of 1.5 arcsec diameter, encompassing the merging galaxies, capture the double peak emission lines, suggesting the presence of a likely dual AGN system.

B is changing direction, supporting the jet precession model leading to the formation of X-shaped radio morphology.

Recall that [B. Sebastian et al. \(2024\)](#) have also examined the reliability of identifying dual AGNs within a sample of six sources exhibiting both an X-shaped radio morphology and double-peaked (DP) emission lines using VLBA observations. Two of those sources, namely, 3C 223.1 and J1430+5217, were in common with the present study but observed at VLBA 4.98 GHz. Among the six targets, three sources, B2 1059+29, J1328+2752, and 4C +61.23, display dual compact components, making them strong candidates for binary black hole (BBH) systems. However, for the remaining three XRGs, J1430+5217, 4C +32.35, and 3C 223.1, the resolved/extended core is seen to extend along the jet direction, suggesting a core-jet configuration.

4.5. Double-peaked XRGs and the role of galaxy merger:

High-resolution hydrodynamical simulations of the NLR regions in the AGNs hosted by merging galaxies suggest the presence of DPNELs in the late stages of the merger ([L. Blecha et al. 2013](#)). Probably only a small fraction of double peaks are directly relatable to the relative motion of the SMBHs, while most originate from complex gas kinematics near the SMBH. Nevertheless, around 80% of these profiles show some influence of SMBH dynamics, manifested as shifted peaks or velocity offsets. Among the merger-induced DPNELs, approximately 10–40% result in SMBH separations in the range of 0.1 to 1 kpc. Furthermore, [P. R. Capelo et al. \(2017\)](#) explored AGN triggering in merging systems by varying parameters such as galaxy mass ratios, orbital configurations, gas content, and black hole properties, concluding

that dual AGNs are found in up to 20–30% of major mergers and 1–10% of minor mergers. This is further supported by [A. Bhattacharya et al. \(2023\)](#), where, using automated techniques, 159 dual AGNs are detected within $z \leq 0.75$ and are mainly associated with red and evolved galaxies, indicating a merger origin. In contrast, the follow-up optical long-slit spectroscopy by [J. M. Comerford et al. \(2018\)](#) of 95 SDSS galaxies exhibiting double-peaked narrow AGN emission lines revealed that only eight sources (<10%) possess companion galaxies with line-of-sight velocity separations below 500 km/s and projected physical separations under 30 kpc.

Given that $\sim 95\%$ of double-peaked emission line XRGs likely host dual AGNs, and considering the galaxy overdensity with similar color in proximity to the central radio source in deep DECaLS images, we shall now briefly explore the role of galaxy mergers in the formation of XRGs. To identify potential mergers, we search for galaxies located near the central radio core that have potential companion matching spectroscopic redshifts within $\Delta z = 0.003$, corresponding to a peculiar velocity of $\sim 1000 \text{ km s}^{-1}$ in small groups ([S. A. Gregory & L. A. Thompson 1978](#); [M. Girardi et al. 1993](#)). Here, we examine galaxies within a 30-arcsecond radius, which corresponds to $\sim 150 \text{ kpc}$ at the average redshift of 0.3, well within the typical virial radius of a central galaxy hosting an AGN. For our sample of 55 DPNEL XRGs, 17 ($\sim 30\%$) exhibit at least one companion galaxy likely indicative of a merger event, whereas 2 XRGs are associated with multiple companion galaxies. The fraction of multiple galaxies rises to $\sim 45\%$ (26/58) if we consider the photo- z selected systems

within $\Delta z = 0.05$. This overdensity around XRGs is further supported by R. Joshi et al. (2019). To assess the clustering environment of XRGs, that study analyzed a sample of 107 sources at $z < 0.4$. The study quantified the number of SDSS galaxies with $M_r \geq -19$ located within a projected radius of 1 Mpc and a redshift interval of $\Delta z = 0.04(1+z)$ around each XRG, and found a median clustering richness of 8.9. The excess merger fraction further suggests that extended NLR sizes derived from the central black hole (Eqn. 2) may possibly be due to the fact that empirical relations may not hold true for merger systems. Interestingly, among the total sample of the 187 XRGs, all five with DPNEL that have deep HST high-resolution images available reveal a close companion and show strong merger signatures with tidal tails (see Figure 8). The SDSS as well as DESI fiber spectra integrate light from both galaxies, resulting in a double-peaked emission profile. This highlights the possible contribution of mergers, which may produce jet reorientation, leading to X-shaped morphology, and making them probable hosts for dual/binary SMBHs as well.

5. CONCLUSIONS

In this study, we performed a systematic search for DPAGNs among 187 XRGs with available SDSS and DESI spectra. Additionally, we report the parsec-scale morphology of the double-peaked XRGs using radio VLBA maps, leading to the following key findings:

1. The XRGs preferentially show a higher (30%) occurrence rate of double-peaked narrow emission lines than the rate of just $\sim 1\%$ found for the general population of galaxies. In addition, the probability of both emission line components in the DPNEL profile exhibiting AGN nature, based on the BPT diagnostic diagram of both [N II] and [S II] lines, is three times higher in XRGs ($\sim 95\%$) than in non-XRGs (30%). This is further corroborated by the MIR color excess in XRGs, yielding an AGN fraction of 91%.
2. The fraction of DPNEL galaxies hosting dual-AGNs is shown to depend strongly on the radio luminosity. This fraction increases from 25% for the radio-undetected to 58% in radio-detected galaxies. The $\sim 95\%$ likelihood of dual AGNs in DPNEL XRGs and also in the radio-powerful DPNEL FR-II radio galaxies suggests the merger-driven scenario for the formation of dual/binary AGNs.
3. The radio core is resolved for one XRG, J2315+1028, in the parsec-scale VLBA maps. The resolved/extended structures are collinear with the jet direction, indicating either a core-jet configuration or a dual AGN scenario. For 5 out of 7 XRGs, the spectral

index between 4 GHz and 8 GHz, ranging from 0.01 to 0.54, indicates a flat spectrum for the VLBA core. The mas-scale radio-optical offset between VLBA and Gaia detections also signifies the presence of multiple cores. In conjunction with both the double-peak emission line components exhibiting an AGN nature, this is strongly indicative of dual/binary AGN.

4. The double-peaked XRGs harbor similar black hole masses and have similar radio luminosities as single-peaked XRGs. We find that more than 30% of DPNEL XRGs have a spectroscopically matched companion galaxy, suggesting that mergers play a substantial role in the formation of X-shaped radio morphology.

ACKNOWLEDGEMENTS

LCH was supported by the National Science Foundation of China (12233001) and the China Manned Space Program (CMS-CSST-2025-A09). SM acknowledges Ramanujan Fellowship (RJF/2020/000113) by DST-ANRF, Govt. of India for this research.

Funding for the Sloan Digital Sky Survey V has been provided by the Alfred P. Sloan Foundation, the Heising-Simons Foundation, the National Science Foundation, and the Participating Institutions. SDSS acknowledges support and resources from the Center for High-Performance Computing at the University of Utah. SDSS telescopes are located at Apache Point Observatory, funded by the Astrophysical Research Consortium and operated by New Mexico State University, and at Las Campanas Observatory, operated by the Carnegie Institution for Science. The SDSS web site is www.sdss.org. SDSS is managed by the Astrophysical Research Consortium for the Participating Institutions of the SDSS Collaboration, including Caltech, The Carnegie Institution for Science, Chilean National Time Allocation Committee (CNTAC) ratified researchers, The Flatiron Institute, the Gotham Participation Group, Harvard University, Heidelberg University, The Johns Hopkins University, L'Ecole polytechnique fédérale de Lausanne (EPFL), Leibniz-Institut für Astrophysik Potsdam (AIP), Max-Planck-Institut für Astronomie (MPIA Heidelberg), Max-Planck-Institut für Extraterrestrische Physik (MPE), Nanjing University, National Astronomical Observatories of China (NAOC), New Mexico State University, The Ohio State University, Pennsylvania State University, Smithsonian Astrophysical Observatory, Space Telescope Science Institute (STScI), the Stellar Astrophysics Participation Group, Universidad Nacional Autónoma de México, University of Arizona, University of Colorado Boulder, University of Illinois at

Urbana-Champaign, University of Toronto, University of Utah, University of Virginia, Yale University, and Yunnan University. The VLBA is operated by the National Radio Astronomy Observatory, a facility of the National Science Foundation operated under cooperative agreement by Associated Universities, Inc. The VLBA observation of 0932+075 at 15.4 GHz carried out on 22 March 2001 was proposed by the CLASS team, specifically by Neal J. Jackson and Martin Norbury. It was devised to be an ultimate proof that

0932+075 was not a GL system. However, the image resulting from that observation has never been published. The raw data belongs to the public domain yet we contacted the proposers and we have received written permission to publish the map resulting from that data in the present paper. This research has made use of the NASA/IPAC Extragalactic Database (NED) which is operated by the Jet Propulsion Laboratory, California Institute of Technology, under contract with the National Aeronautics and Space Administration. DECaLS, SDSS, VLBA, NVSS and WISE

REFERENCES

- Abdurro'uf, Lin, Y.-T., Wu, P.-F., & Akiyama, M. 2021, *ApJS*, 254, 15, doi: [10.3847/1538-4365/abebe2](https://doi.org/10.3847/1538-4365/abebe2)
- Ahumada, R., Allende Prieto, C., Almeida, A., et al. 2020, *ApJS*, 249, 3, doi: [10.3847/1538-4365/ab929e](https://doi.org/10.3847/1538-4365/ab929e)
- Aihara, H., Allende Prieto, C., An, D., et al. 2011, *ApJS*, 193, 29, doi: [10.1088/0067-0049/193/2/29](https://doi.org/10.1088/0067-0049/193/2/29)
- Almeida, A., Anderson, S. F., Argudo-Fernández, M., et al. 2023, *ApJS*, 267, 44, doi: [10.3847/1538-4365/acda98](https://doi.org/10.3847/1538-4365/acda98)
- Amaro-Seoane, P., Audley, H., Babak, S., et al. 2017, *arXiv e-prints*, arXiv:1702.00786, doi: [10.48550/arXiv.1702.00786](https://doi.org/10.48550/arXiv.1702.00786)
- Babul, A., Sharma, P., & Reynolds, C. S. 2013, *ApJ*, 768, 11, doi: [10.1088/0004-637X/768/1/11](https://doi.org/10.1088/0004-637X/768/1/11)
- Baldwin, J. A., Phillips, M. M., & Terlevich, R. 1981, *PASP*, 93, 5, doi: [10.1086/130766](https://doi.org/10.1086/130766)
- Becker, R. H., White, R. L., & Edwards, A. L. 1995, *VizieR Online Data Catalog: A new catalog of 53522 4.85GHz sources (Becker+ 1991),, VizieR On-line Data Catalog: VIII/13. Originally published in: 1991ApJS...75....1B*
- Begelman, M. C., Blandford, R. D., & Rees, M. J. 1980, *Nature*, 287, 307, doi: [10.1038/287307a0](https://doi.org/10.1038/287307a0)
- Bera, S., Pal, S., Sasmal, T. K., & Mondal, S. 2020, *ApJS*, 251, 9, doi: [10.3847/1538-4365/abb367](https://doi.org/10.3847/1538-4365/abb367)
- Bhattacharya, A., Nehal, C. P., Das, M., et al. 2023, *MNRAS*, 524, 4482, doi: [10.1093/mnras/stad2117](https://doi.org/10.1093/mnras/stad2117)
- Blecha, L., Loeb, A., & Narayan, R. 2013, *MNRAS*, 429, 2594, doi: [10.1093/mnras/sts533](https://doi.org/10.1093/mnras/sts533)
- Bon, E., Jovanović, P., Marziani, P., et al. 2012, *ApJ*, 759, 118, doi: [10.1088/0004-637X/759/2/118](https://doi.org/10.1088/0004-637X/759/2/118)
- Capelo, P. R., Dotti, M., Volonteri, M., et al. 2017, *MNRAS*, 469, 4437, doi: [10.1093/mnras/stx1067](https://doi.org/10.1093/mnras/stx1067)
- Cappellari, M. 2023, *MNRAS*, 526, 3273, doi: [10.1093/mnras/stad2597](https://doi.org/10.1093/mnras/stad2597)
- Carnall, A. C., McLure, R. J., Dunlop, J. S., & Davé, R. 2018, *MNRAS*, 480, 4379, doi: [10.1093/mnras/sty2169](https://doi.org/10.1093/mnras/sty2169)
- Chabrier, G. 2003, *PASP*, 115, 763, doi: [10.1086/376392](https://doi.org/10.1086/376392)
- Charlot, S., & Fall, S. M. 2000, *ApJ*, 539, 718, doi: [10.1086/309250](https://doi.org/10.1086/309250)
- Chen, Y.-C., Liu, X., Lazio, J., et al. 2023, *ApJ*, 958, 29, doi: [10.3847/1538-4357/ad00b3](https://doi.org/10.3847/1538-4357/ad00b3)
- Cheung, C. C. 2007, *AJ*, 133, 2097, doi: [10.1086/513095](https://doi.org/10.1086/513095)
- Cigan, P., Makarov, V. V., Secrest, N. J., et al. 2024, *ApJS*, 274, 28, doi: [10.3847/1538-4365/ad6772](https://doi.org/10.3847/1538-4365/ad6772)
- Collaboration, D., Abdul-Karim, M., Adame, A. G., et al. 2025, *Data Release 1 of the Dark Energy Spectroscopic Instrument*, <https://arxiv.org/abs/2503.14745>
- Comerford, J. M., Nevin, R., Stemo, A., et al. 2018, *ApJ*, 867, 66, doi: [10.3847/1538-4357/aae2b4](https://doi.org/10.3847/1538-4357/aae2b4)
- Comerford, J. M., Pooley, D., Barrows, R. S., et al. 2015, *ApJ*, 806, 219, doi: [10.1088/0004-637X/806/2/219](https://doi.org/10.1088/0004-637X/806/2/219)
- Condon, J. J., Cotton, W. D., Greisen, E. W., et al. 1998, *AJ*, 115, 1693, doi: [10.1086/300337](https://doi.org/10.1086/300337)
- Coziol, R., Torres-Papaqui, J. P., & Andernach, H. 2015, *AJ*, 149, 192, doi: [10.1088/0004-6256/149/6/192](https://doi.org/10.1088/0004-6256/149/6/192)
- De Rosa, A., Vignali, C., Bogdanović, T., et al. 2019, *NewAR*, 86, 101525, doi: [10.1016/j.newar.2020.101525](https://doi.org/10.1016/j.newar.2020.101525)
- Deller, A. T., Brisken, W. F., Phillips, C. J., et al. 2011, *PASP*, 123, 275, doi: [10.1086/658907](https://doi.org/10.1086/658907)
- Dennett-Thorpe, J., Scheuer, P. A. G., Laing, R. A., et al. 2002, *MNRAS*, 330, 609, doi: [10.1046/j.1365-8711.2002.05106.x](https://doi.org/10.1046/j.1365-8711.2002.05106.x)
- Doan, A., Eracleous, M., Runnoe, J. C., et al. 2020, *MNRAS*, 491, 1104, doi: [10.1093/mnras/stz2705](https://doi.org/10.1093/mnras/stz2705)
- Draine, B. T., & Li, A. 2007, *ApJ*, 657, 810, doi: [10.1086/511055](https://doi.org/10.1086/511055)
- Efstathiou, G., & Silk, J. 1983, *FCPh*, 9, 1
- Fanaroff, B. L., & Riley, J. M. 1974, *MNRAS*, 167, 31P
- Fitzpatrick, E. L. 1999, *PASP*, 111, 63, doi: [10.1086/316293](https://doi.org/10.1086/316293)
- Frenk, C. S., White, S. D. M., Davis, M., & Efstathiou, G. 1988, *ApJ*, 327, 507, doi: [10.1086/166213](https://doi.org/10.1086/166213)
- Fu, H., Myers, A. D., Djorgovski, S. G., & Yan, L. 2011, *ApJ*, 733, 103, doi: [10.1088/0004-637X/733/2/103](https://doi.org/10.1088/0004-637X/733/2/103)
- Gaia Collaboration, Vallenari, A., Brown, A. G. A., et al. 2023, *A&A*, 674, A1, doi: [10.1051/0004-6361/202243940](https://doi.org/10.1051/0004-6361/202243940)

- Ge, J.-Q., Hu, C., Wang, J.-M., Bai, J.-M., & Zhang, S. 2012, *ApJS*, 201, 31, doi: [10.1088/0067-0049/201/2/31](https://doi.org/10.1088/0067-0049/201/2/31)
- Gehrels, N. 1986, *ApJ*, 303, 336, doi: [10.1086/164079](https://doi.org/10.1086/164079)
- Girardi, M., Biviano, A., Giuricin, G., Mardirossian, F., & Mezzetti, M. 1993, *ApJ*, 404, 38, doi: [10.1086/172256](https://doi.org/10.1086/172256)
- Giri, G., Fendt, C., Thorat, K., Bodo, G., & Rossi, P. 2024, *Frontiers in Astronomy and Space Sciences*, 11, 1371101, doi: [10.3389/fspas.2024.1371101](https://doi.org/10.3389/fspas.2024.1371101)
- Gopal-Krishna, Biermann, P. L., Gergely, L. Á., & Wiita, P. J. 2012, *Research in Astronomy and Astrophysics*, 12, 127, doi: [10.1088/1674-4527/12/2/002](https://doi.org/10.1088/1674-4527/12/2/002)
- Gopal-Krishna, Biermann, P. L., & Wiita, P. J. 2003, *ApJL*, 594, L103, doi: [10.1086/378766](https://doi.org/10.1086/378766)
- Gopal Krishna, & Dabhade, P. 2022, *A&A*, 663, L8, doi: [10.1051/0004-6361/202244113](https://doi.org/10.1051/0004-6361/202244113)
- Gopal-Krishna, & Wiita, P. J. 2000, *A&A*, 363, 507, doi: [10.48550/arXiv.astro-ph/0009441](https://doi.org/10.48550/arXiv.astro-ph/0009441)
- Graham, M. J., Djorgovski, S. G., Stern, D., et al. 2015, *Nature*, 518, 74, doi: [10.1038/nature14143](https://doi.org/10.1038/nature14143)
- Greene, J. E., Strader, J., & Ho, L. C. 2020, *ARA&A*, 58, 257, doi: [10.1146/annurev-astro-032620-021835](https://doi.org/10.1146/annurev-astro-032620-021835)
- Gregory, S. A., & Thompson, L. A. 1978, *ApJ*, 222, 784, doi: [10.1086/156198](https://doi.org/10.1086/156198)
- Greisen, E. W. 2003, *Astrophysics and Space Science Library*, Vol. 285, AIPS, the VLA, and the VLBA, 109, doi: [10.1007/0-306-48080-8_7](https://doi.org/10.1007/0-306-48080-8_7)
- Guo, H., Shen, Y., & Wang, S. 2018, *PyQSOFit: Python code to fit the spectrum of quasars*, *Astrophysics Source Code Library*, record ascl:1809.008
- Hernquist, L. 1989, *Nature*, 340, 687, doi: [10.1038/340687a0](https://doi.org/10.1038/340687a0)
- Hopkins, P. F., Hernquist, L., Cox, T. J., et al. 2006a, *ApJS*, 163, 1, doi: [10.1086/499298](https://doi.org/10.1086/499298)
- Hopkins, P. F., Somerville, R. S., Hernquist, L., et al. 2006b, *ApJ*, 652, 864, doi: [10.1086/508503](https://doi.org/10.1086/508503)
- Hou, M., Liu, X., Guo, H., et al. 2019, *ApJ*, 882, 41, doi: [10.3847/1538-4357/ab3225](https://doi.org/10.3847/1538-4357/ab3225)
- Imanishi, M., & Saito, Y. 2014, *ApJ*, 780, 106, doi: [10.1088/0004-637X/780/1/106](https://doi.org/10.1088/0004-637X/780/1/106)
- Joshi, R., Srianand, R., Noterdaeme, P., & Petitjean, P. 2017, *MNRAS*, 465, 701, doi: [10.1093/mnras/stw2733](https://doi.org/10.1093/mnras/stw2733)
- Joshi, R., Krishna, G., Yang, X., et al. 2019, *ApJ*, 887, 266, doi: [10.3847/1538-4357/ab536f](https://doi.org/10.3847/1538-4357/ab536f)
- Kauffmann, G., & Haehnelt, M. 2000, *MNRAS*, 311, 576, doi: [10.1046/j.1365-8711.2000.03077.x](https://doi.org/10.1046/j.1365-8711.2000.03077.x)
- Kauffmann, G., Heckman, T. M., Tremonti, C., et al. 2003, *MNRAS*, 346, 1055, doi: [10.1111/j.1365-2966.2003.07154.x](https://doi.org/10.1111/j.1365-2966.2003.07154.x)
- Kewley, L. J., Dopita, M. A., Sutherland, R. S., Heisler, C. A., & Trevena, J. 2001, *ApJ*, 556, 121, doi: [10.1086/321545](https://doi.org/10.1086/321545)
- Kewley, L. J., Groves, B., Kauffmann, G., & Heckman, T. 2006, *MNRAS*, 372, 961, doi: [10.1111/j.1365-2966.2006.10859.x](https://doi.org/10.1111/j.1365-2966.2006.10859.x)
- Kharb, P., Lal, D. V., & Merritt, D. 2017, *Nature Astronomy*, 1, 727, doi: [10.1038/s41550-017-0256-4](https://doi.org/10.1038/s41550-017-0256-4)
- Komossa, S. 2006, *Mem. Soc. Astron. Italiana*, 77, 733
- Kormendy, J., & Ho, L. C. 2013, *Annual Review of Astronomy and Astrophysics*, 51, 511, doi: [10.1146/annurev-astro-082708-101811](https://doi.org/10.1146/annurev-astro-082708-101811)
- Kovalev, Y. Y., Petrov, L., & Plavin, A. V. 2017, *A&A*, 598, L1, doi: [10.1051/0004-6361/201630031](https://doi.org/10.1051/0004-6361/201630031)
- Lacy, M., Storrie-Lombardi, L. J., Sajina, A., et al. 2004, *ApJS*, 154, 166, doi: [10.1086/422816](https://doi.org/10.1086/422816)
- Landt, H., Cheung, C. C., & Healey, S. E. 2010, *MNRAS*, 408, 1103, doi: [10.1111/j.1365-2966.2010.17183.x](https://doi.org/10.1111/j.1365-2966.2010.17183.x)
- Lao, B.-Q., Yang, X.-L., Jaiswal, S., et al. 2024, *Research in Astronomy and Astrophysics*, 24, 035021, doi: [10.1088/1674-4527/ad204f](https://doi.org/10.1088/1674-4527/ad204f)
- Liddle, A. R. 2007, *MNRAS*, 377, L74, doi: [10.1111/j.1745-3933.2007.00306.x](https://doi.org/10.1111/j.1745-3933.2007.00306.x)
- Liu, X., Civano, F., Shen, Y., et al. 2013, *ApJ*, 762, 110, doi: [10.1088/0004-637X/762/2/110](https://doi.org/10.1088/0004-637X/762/2/110)
- Liu, X., Guo, H., Shen, Y., Greene, J. E., & Strauss, M. A. 2018, *ApJ*, 862, 29, doi: [10.3847/1538-4357/aac9cb](https://doi.org/10.3847/1538-4357/aac9cb)
- Maschmann, D., Melchior, A.-L., Mamon, G. A., Chilingarian, I. V., & Katkov, I. Y. 2020, *A&A*, 641, A171, doi: [10.1051/0004-6361/202037868](https://doi.org/10.1051/0004-6361/202037868)
- McGurk, R. C., Max, C. E., Medling, A. M., Shields, G. A., & Comerford, J. M. 2015, *ApJ*, 811, 14, doi: [10.1088/0004-637X/811/1/14](https://doi.org/10.1088/0004-637X/811/1/14)
- Merritt, D., & Ekers, R. D. 2002, *Science*, 297, 1310, doi: [10.1126/science.1074688](https://doi.org/10.1126/science.1074688)
- Mezcua, M., Lobanov, A. P., Chavushyan, V. H., & León-Tavares, J. 2011, *A&A*, 527, A38, doi: [10.1051/0004-6361/201015535](https://doi.org/10.1051/0004-6361/201015535)
- Müller-Sánchez, F., Comerford, J. M., Nevin, R., et al. 2015, *ApJ*, 813, 103, doi: [10.1088/0004-637X/813/2/103](https://doi.org/10.1088/0004-637X/813/2/103)
- Nenkova, M., Sirocky, M. M., Ivezić, Ž., & Elitzur, M. 2008a, *ApJ*, 685, 147, doi: [10.1086/590482](https://doi.org/10.1086/590482)
- Nenkova, M., Sirocky, M. M., Nikutta, R., Ivezić, Ž., & Elitzur, M. 2008b, *ApJ*, 685, 160, doi: [10.1086/590483](https://doi.org/10.1086/590483)
- Nevin, R., Comerford, J., Müller-Sánchez, F., Barrows, R., & Cooper, M. 2016, *ApJ*, 832, 67, doi: [10.3847/0004-637X/832/1/67](https://doi.org/10.3847/0004-637X/832/1/67)
- Newville, M., Otten, R., Nelson, A., et al. 2024, *lmfit/lmfit-py*: 1.3.2, 1.3.2 Zenodo, doi: [10.5281/zenodo.598352](https://doi.org/10.5281/zenodo.598352)
- O'Neill, S., Kiehlmann, S., Readhead, A. C. S., et al. 2022, *ApJL*, 926, L35, doi: [10.3847/2041-8213/ac504b](https://doi.org/10.3847/2041-8213/ac504b)
- Orosz, G., & Frey, S. 2013, *A&A*, 553, A13, doi: [10.1051/0004-6361/201321279](https://doi.org/10.1051/0004-6361/201321279)
- Osterbrock, D. E., & Ferland, G. J. 2006, *Astrophysics of gaseous nebulae and active galactic nuclei*
- Perna, M., Arribas, S., Marshall, M., et al. 2023, *A&A*, 679, A89, doi: [10.1051/0004-6361/202346649](https://doi.org/10.1051/0004-6361/202346649)

- Petrov, L. Y., & Kovalev, Y. Y. 2025, VizieR Online Data Catalog: The Radio Fundamental Catalog - RFC (Petrov+, 2025), VizieR On-line Data Catalog: J/ApJS/276/38. Originally published in: 2025ApJS..276...38P
- Pfeifle, R. W., Weaver, K. A., Secrest, N. J., Rothberg, B., & Patton, D. R. 2024, arXiv e-prints, arXiv:2411.12799, doi: [10.48550/arXiv.2411.12799](https://doi.org/10.48550/arXiv.2411.12799)
- Plavin, A. V., Kovalev, Y. Y., Pushkarev, A. B., & Lobanov, A. P. 2019, MNRAS, 485, 1822, doi: [10.1093/mnras/stz504](https://doi.org/10.1093/mnras/stz504)
- Proctor, D. D. 2011, ApJS, 194, 31, doi: [10.1088/0067-0049/194/2/31](https://doi.org/10.1088/0067-0049/194/2/31)
- Puerto-Sánchez, C., Habouzit, M., Volonteri, M., et al. 2025, MNRAS, 536, 3016, doi: [10.1093/mnras/stae2763](https://doi.org/10.1093/mnras/stae2763)
- Ren, W., Guo, H., Shen, Y., et al. 2024, ApJ, 974, 153, doi: [10.3847/1538-4357/ad6e76](https://doi.org/10.3847/1538-4357/ad6e76)
- Rodriguez, C., Taylor, G. B., Zavala, R. T., et al. 2006, ApJ, 646, 49, doi: [10.1086/504825](https://doi.org/10.1086/504825)
- Rottmann, H. 2002, PhD thesis, Rheinische Friedrich Wilhelms University of Bonn, Germany
- Rubinur, K., Das, M., & Kharb, P. 2019, MNRAS, 484, 4933, doi: [10.1093/mnras/stz334](https://doi.org/10.1093/mnras/stz334)
- Rubinur, K., Das, M., Kharb, P., & Honey, M. 2017, MNRAS, 465, 4772, doi: [10.1093/mnras/stw2981](https://doi.org/10.1093/mnras/stw2981)
- Schlaflly, E. F., Meisner, A. M., & Green, G. M. 2019, ApJS, 240, 30, doi: [10.3847/1538-4365/aafbea](https://doi.org/10.3847/1538-4365/aafbea)
- Schwartzman, E., Clarke, T. E., Nyland, K., et al. 2024, ApJ, 961, 233, doi: [10.3847/1538-4357/ad0ed0](https://doi.org/10.3847/1538-4357/ad0ed0)
- Schwarz, G. 1978, Annals of Statistics, 6, 461
- Scialpi, M., Mannucci, F., Marconcini, C., et al. 2024, A&A, 690, A57, doi: [10.1051/0004-6361/202347242](https://doi.org/10.1051/0004-6361/202347242)
- Sebastian, B., Caproni, A., Kharb, P., et al. 2024, MNRAS, 530, 4902, doi: [10.1093/mnras/stae546](https://doi.org/10.1093/mnras/stae546)
- Severgnini, P., Braitto, V., Ciccone, C., et al. 2021, A&A, 646, A153, doi: [10.1051/0004-6361/202039576](https://doi.org/10.1051/0004-6361/202039576)
- Shangguan, J., Liu, X., Ho, L. C., et al. 2016, ApJ, 823, 50, doi: [10.3847/0004-637X/823/1/50](https://doi.org/10.3847/0004-637X/823/1/50)
- Shimwell, T. W., Hardcastle, M. J., Tasse, C., et al. 2022, A&A, 659, A1, doi: [10.1051/0004-6361/202142484](https://doi.org/10.1051/0004-6361/202142484)
- Siudek, M., Pucha, R., Mezcuca, M., et al. 2024, A&A, 691, A308, doi: [10.1051/0004-6361/202451761](https://doi.org/10.1051/0004-6361/202451761)
- Smith, K. L., Shields, G. A., Bonning, E. W., et al. 2010, ApJ, 716, 866, doi: [10.1088/0004-637X/716/1/866](https://doi.org/10.1088/0004-637X/716/1/866)
- Sokolovsky, K. V., Kovalev, Y. Y., Pushkarev, A. B., & Lobanov, A. P. 2011, A&A, 532, A38, doi: [10.1051/0004-6361/201016072](https://doi.org/10.1051/0004-6361/201016072)
- Stern, D., Eisenhardt, P., Gorjian, V., et al. 2005, ApJ, 631, 163, doi: [10.1086/432523](https://doi.org/10.1086/432523)
- Tang, S., & Grindlay, J. 2009, ApJ, 704, 1189, doi: [10.1088/0004-637X/704/2/1189](https://doi.org/10.1088/0004-637X/704/2/1189)
- Vazdekis, A., Sánchez-Blázquez, P., Falcón-Barroso, J., et al. 2010, MNRAS, 404, 1639, doi: [10.1111/j.1365-2966.2010.16407.x](https://doi.org/10.1111/j.1365-2966.2010.16407.x)
- Villforth, C., & Hamann, F. 2015, AJ, 149, 92, doi: [10.1088/0004-6256/149/3/92](https://doi.org/10.1088/0004-6256/149/3/92)
- Volonteri, M., Haardt, F., & Madau, P. 2003, ApJ, 582, 559, doi: [10.1086/344675](https://doi.org/10.1086/344675)
- Wang, J.-M., Chen, Y.-M., Hu, C., et al. 2009, ApJL, 705, L76, doi: [10.1088/0004-637X/705/1/L76](https://doi.org/10.1088/0004-637X/705/1/L76)
- White, S. D. M., & Rees, M. J. 1978, MNRAS, 183, 341, doi: [10.1093/mnras/183.3.341](https://doi.org/10.1093/mnras/183.3.341)
- Wright, E. L., Eisenhardt, P. R. M., Mainzer, A. K., et al. 2010, AJ, 140, 1868, doi: [10.1088/0004-6256/140/6/1868](https://doi.org/10.1088/0004-6256/140/6/1868)
- Xu, D., & Komossa, S. 2009, ApJL, 705, L20, doi: [10.1088/0004-637X/705/1/L20](https://doi.org/10.1088/0004-637X/705/1/L20)
- Xu, W., Cui, L., Liu, X., et al. 2024, ApJ, 969, 36, doi: [10.3847/1538-4357/ad463b](https://doi.org/10.3847/1538-4357/ad463b)
- Yang, X., Joshi, R., Gopal-Krishna, et al. 2019, ApJS, 245, 17, doi: [10.3847/1538-4365/ab4811](https://doi.org/10.3847/1538-4365/ab4811)
- Yang, X., Ji, J., Joshi, R., et al. 2022, ApJ, 933, 98, doi: [10.3847/1538-4357/ac71aa](https://doi.org/10.3847/1538-4357/ac71aa)
- Zhang, X.-G., Dultzin-Hacyan, D., & Wang, T.-G. 2007, MNRAS, 377, 1215, doi: [10.1111/j.1365-2966.2007.11673.x](https://doi.org/10.1111/j.1365-2966.2007.11673.x)
- Zhang, Y.-W., Huang, Y., Bai, J.-M., et al. 2021, AJ, 162, 289, doi: [10.3847/1538-3881/ac2deb](https://doi.org/10.3847/1538-3881/ac2deb)
- Zier, C., & Biermann, P. L. 2001, A&A, 377, 23, doi: [10.1051/0004-6361:20010862](https://doi.org/10.1051/0004-6361:20010862)